water

MDPI

Article

A Probabilistic Approach for Off-Stream Reservoir Failure Flood Hazard Assessment

Marcos Sanz-Ramos [1,*], Ernest Bladé [1], Nathalia Silva-Cancino [2], Fernando Salazar [2], David López-Gómez [3] and Eduardo Martínez-Gomariz [1,4]

[1] Flumen Research Institute, Universitat Politècnica de Catalunya (UPC)—Centre Internacional de Mètodes Numèrics en Enginyeria (CIMNE), 08034 Barcelona, Spain; ernest.blade@upc.edu (E.B.); eduardo.martinez-gomariz@upc.edu (E.M.-G.)
[2] Centre Internacional de Mètodes Numèrics en Enginyeria (CIMNE), 08034 Barcelona, Spain; nsilva@cimne.upc.edu (N.S.-C.); fsalazar@cimne.upc.edu (F.S.)
[3] Centro de Estudios Hidrográficos, Centro de Estudios y Experimentación de Obras Públicas (CEDEX), 28005 Madrid, Spain; david.lopez@cedex.es
[4] Innovation and Knowledge Department, Aigües de Barcelona, 08028 Barcelona, Spain
* Correspondence: marcos.sanz-ramos@upc.edu; Tel.: +34-93-405-42-51

Abstract: Off-stream reservoirs are hydraulic structures that might cause severe flood damages in case of failure or improper operation. Their safety regulations usually require hydraulic studies for flood hazard and inundation zone mapping. The selection of the break point is not trivial because the topography in its surroundings is commonly highly anthropic. A wrong selection would not provide the worst scenario in terms of maximum flood hazard extent. This work presents a probabilistic approach based on a stochastic definition of the break point along the dyke. A number of failure scenarios are generated automatically, corresponding to different breach formations. Then, an in-cascade calculation process simulates each scenario, providing a framework to carry out statistical analysis. The simulation of the breach formation and the flood wave propagation is performed through a GPU parallelised two-dimensional hydraulic numerical model, which provides a probabilistic inundation zone and flood hazard mapping of all scenarios simulated in a suitable timeframe.

Keywords: off-stream reservoir; statistical analysis; probabilistic flood mapping; Iber

Citation: Sanz-Ramos, M.; Bladé, E.; Silva-Cancino, N.; Salazar, F.; López-Gómez, D.; Martínez-Gomariz, E. A Probabilistic Approach for Off-Stream Reservoir Failure Flood Hazard Assessment. *Water* **2023**, *15*, 2202. https://doi.org/10.3390/w15122202

Academic Editors: Bommanna Krishnappan and Oz Sahin

Received: 8 May 2023
Revised: 30 May 2023
Accepted: 9 June 2023
Published: 12 June 2023

1. Introduction

Floods are natural phenomena that cause serious economic, environmental and social damage [1,2]. However, in certain situations, floods can be induced by anthropic actions [3–7]. In such cases, the flood risk become greater not only due to the increase in vulnerability and exposure [8–11], but also when a wrong operation or malfunctioning of flood protection structures may occur [12–18]. This is, for example, the case for the eventual failure or improper operation of hydraulic structures such as dams, off-stream reservoirs, levees, irrigations channels, etc.

Off-stream reservoirs are defined as human-made structures designed for the storage of any kind of fluid—usually water and mine tailings—located outside the basin's channel network and totally or partially delimited by a retention dyke. They are essential structures for different purposes, such as: water supply to small populations, irrigation, cattle raising, firefighting, purification, recreation, mine tailings, and electric facilities, among other uses [19–23].

Accounting for the similarities with dams, off-stream reservoirs are commonly treated as dams and the same safety regulatory regime commonly applies. Thus, off-stream reservoirs are often classified into various categories according to safety requirements adopting different formulations in several countries [24].

To that end, hydraulic studies that consider the break of the dyke of the structure, and the subsequent flood wave propagation, are utilised for flood hazard and inundation extent mapping. Flood risk management and emergency response planning are among the flood mitigation measures to minimise property damage and loss of life [25,26]. These studies serve as the basis for the classification process to determine the potential risk that a flood might cause to the elements at risk located in the vicinity of the structure. Several numerical tools are available for practitioners to simulate the breach formation on dams or off-stream reservoirs (DAMBRK, SMPDBK, FLDWAV, Iber, FLO-2D, etc.) and, thus, the subsequent flood wave propagation process (INFOWORKS, HEC-RAS, Iber, FLO-2D, GUAD 2D, etc.).

One of the main issues when practitioners deal with the classification of an off-stream reservoir according to their potential damage in case of failure or improper operation is the selection of the break point. In case of dams, there is generally no subjectivity on the selection of this point: the worse situation is a break at the tallest part of the dam, which usually coincides with the river. However, the selection of this point is not trivial in off-stream reservoirs because they are not directly associated to a river bed and may have irregular geometry.

Off-stream reservoirs are usually built near agricultural fields or mining facilities, being the terrain notably modified with several anthropic actions (smoothing slopes, changing the natural drainage network, conforming terraces, etc.). As a result, the flood wave propagation process is complex and, at first instance, not easily determinable. An analysis considering only a single break point (a simulation scenario) could lead to an underestimation of potential damages because the break point that would cause the worst potential damages is generally unknown. To solve this issue, practitioners traditionally analyse several break scenarios according, for example, to the number of dykes of the off-stream reservoir or to topographical aspects. Despite that, the worst break point might not be selected and, thus, it would result, again, in an underestimation of the maximum potential damages.

In such cases, a deterministic approach might not be sufficiently suitable. Several flood studies focus the flood hazard analysis from a statistical point of view. Ahmadisharaf et al. [27] used the outflow hydrograph as the uncertain parameter in a Monte-Carlo-based probabilistic approach. Rizzo et al. [28] analysed the influence of the breach width and the reservoir level before the breach formation. The study of Bello et al. [29] also deal with the influence of the breach parameters in the generation of the hydrograph. All of them focus on dam-like structures and the parameters for the breach definition, while probabilistic off-stream reservoir flood hazard studies are less analysed in the bibliography.

The present study aims to fill this gap with a probabilistic approach for off-stream reservoir failure flood hazard assessment. The breach parameters are kept unchanged, while the break point is defined stochastically along the dyke of the structure. Each breach formation and the flood wave propagation are simulated in the same model following an in-cascade process. Then, the hydraulic results are analysed statistically to generate probabilistic flood extent and flood hazard maps. The whole process was integrated in a unique numerical tool, providing to practitioners the results of each deterministic scenario, the possibility to carry out a probabilistic approach for flood hazard assessment based on them, and the direct determination of the envelope of the flood extent. Additionally, the proposed methodology allowed for exploring the minimum number of scenarios necessary to provide good statistical results and exploring how the computational domain can be optimised.

2. Materials and Methods

2.1. Breach Formation and Flood Propagation Modelling

Iber is a software that solves 2D depth-averaged shallow water equations using a finite volume solver [30,31]. It includes, among other calculation modules and capabilities [15,32–39], a specific tool that considers the breach formation in the simulation

process. Thus, this numerical tool can simulate, jointly, the generation of a breach in a dyke and the subsequent propagation of the flood in the calculation domain.

Iber implements two types of breaches, both trapezoidal-shaped. One follows the specifications of the Spanish Technical Guide [40], whose section is defined as a trapezium of 1/1 lateral slope. The time formation (T_f) and average width (b_{avg}) of the breach are calculated as follows:

$$T_f = 4.8\frac{\sqrt{V}}{H} \quad (1)$$

$$b_{avg} = 20(VH)^{0.25} \quad (2)$$

where V is the volume of the reservoir (in hm^3) and H is the height of the dyke measured from the crest to the terrain (in m). The other methodology follows the user's specifications, i.e., the breach is defined by the top (b_t) and bottom (b_b) width, the top (z_t) and bottom (z_b) elevation, and the time formation (T_f). Thus, the user also manages the lateral slope (S) of the breach (Figure 1a).

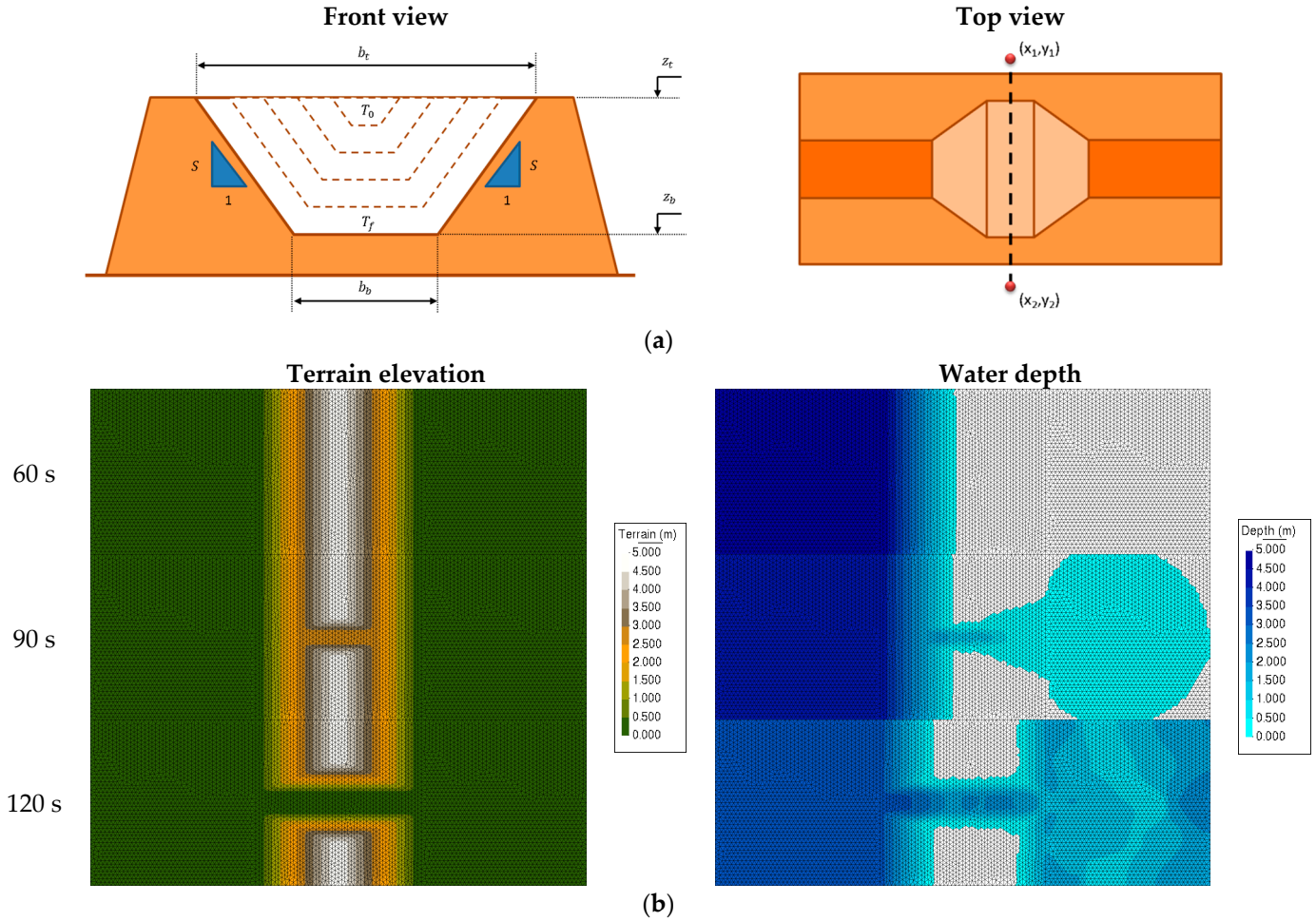

Figure 1. (**a**) Sketch of a breach formation process in a dyke as modelled by Iber. (**b**) Breach formation according to user's specifications (**left**): b_t = 5 m, b_b = 2 m, z_t = 5 m z_b = 0 m, T_0 = 60 s, and T_f = 60 s. Flood propagation caused by the opening in the dyke (**right**).

Once a breach is activated in the model, the terrain evolves, generating a trapezoidal-shaped section along a generatrix axis (Figure 1a). The breach formation process can start when either the simulation time (T_0) or the water elevation (WE_0) on the inner part of the dyke is greater than a particular value defined by the user. This latter option is designed for the generation of breaches caused by overtopping, dams' main failure mode [41], but

it can be also used for off-stream reservoirs if endogenous rainfall is considered or if malfunctioning of the filling system is produced.

The breach formation is considered in the model numerically. During the simulation, Iber changes the elevation of the nodes of the calculation mesh according to the breach specifications. Once the elevation of the nodes is lower than the water elevation, the fluid leaves the reservoir. Figure 1b exemplifies the breach formation process (left) and the consequences on the fluid motion (right), which is originally at rest at one side of the dyke (T_0 = 60 s).

Currently, the whole calculation process can be performed with the sequential version, using the computing processor unit (CPU), or with the parallelized version, which uses the graphical processor unit (GPU), called R-Iber [35]. The breach formation process described above has been incorporated into this new parallelized code, allowing to reach speed-ups above 80 in comparison to the sequential version.

2.2. Stochastic Breach Generation and Probabilistic Approach

The present probabilistic approach for off-stream reservoir failure flood hazard assessment is based on a stochastic definition of the break points along the dyke. Instead of analysing each scenario separately, as in a deterministic approach, a large number of simulations are automatically carried out in the same model allowing, then, a probabilistic analysis.

To that end, once the crest of the dyke is selected (Figure 2a, red dashed line) the breaches are automatically generated separated by an equidistance (Figure 2a, white lines). The parameters of the breach defined by the user (kind of breach, top/bottom elevation, top/bottom width, time formation, etc.) are also applied automatically. Thereby, a number of failure scenarios will be generated automatically, corresponding each one to a breach formation. Following this, an in-cascade calculation process simulates each scenario and saves the results in the same model (Figure 2b).

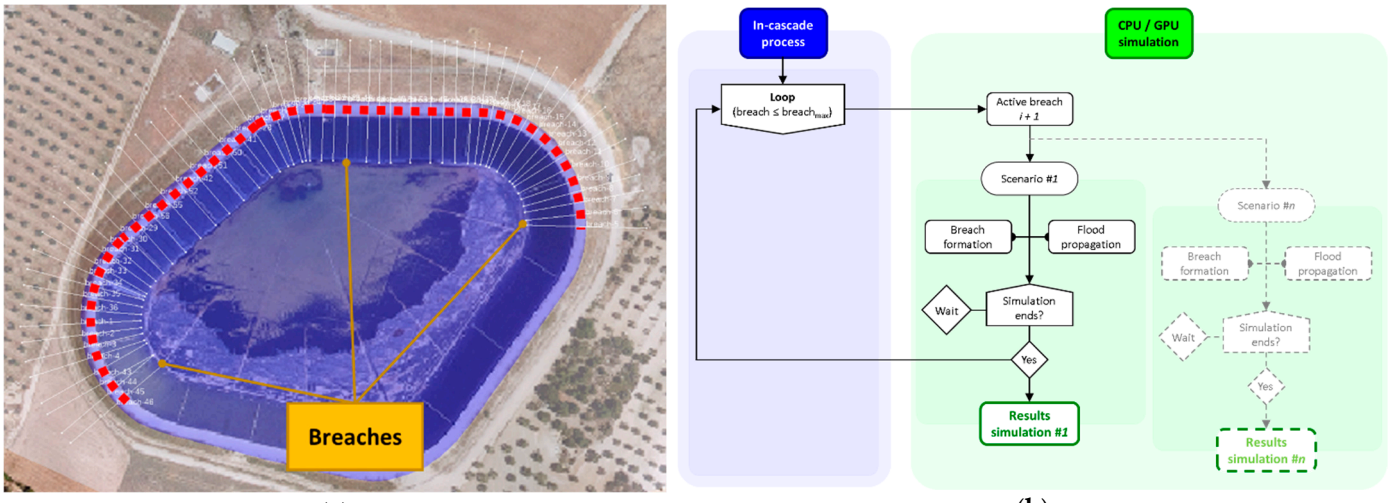

(**a**) (**b**)

Figure 2. (**a**) Example of automatic breach generation (56 breaches, white alignments) according to the selection of the crest of the dyke (red dashed line). (**b**) General flow chart of the code for the *n* scenarios calculated with an in-cascade computation process.

Any numerical tool can run several simulations at the same time in the same processor unit. However, this creates a significant bottleneck, reducing the global computing capacity, especially when a GPU device is utilised [42]. Despite R-Iber allowing the selection of the GPU device on which to carry out each simulation [35], the use of either a cluster of GPUs or CPUs by practitioners is infrequent. For this reason, an in-cascade simulation process was selected instead of a parallel simulation process (a simulation per device). This

procedure allows for the comparison of the calculation time between the sequential and parallelised versions.

Once the simulation ends, the results of all scenarios can be loaded into the interface and jointly analysed. On one hand, a deterministic analysis can be performed scenario per scenario, as traditionally carried out, looking for the breach (or scenario) that provides the worst potential damages. On the other hand, if the number of scenarios is large enough, a probabilistic approach is recommended for the results analysis.

For this last purpose, a new tool was developed, allowing the user to select the threshold for the hydraulic variables (depth, velocity, specific discharge, and water elevation) and the hazard criteria of any existing recommendations or guide. This tool evaluates whether the threshold is exceeded in any element of the calculation domain and scenario. In the affirmative case, class 1 is assigned to the element. Accounting for the number of class 1 of each element in all scenarios, the probability of exceedance of a particular threshold is directly obtained at each element. Thereby, flood probability maps are automatically generated with this methodology.

The presented methodology is independent of the type of fluid stored in the off-stream reservoir. Despite it not only being applied to irrigation ponds (water, "Newtonian" fluid-like), there is no limitations to use it, for example, in mine tailing ponds (muds, non-Newtonian fluid-like). This approach can help in the development of ad hoc guidelines that allow the complexity of fluid, tailings, and dam failures to be considered in order to properly characterize potential breach and runout scenarios [20,43].

2.3. Case Studies

The performance of the probabilistic approach was tested in four case studies located in Spain (Figure 3). The Rubial case study is a structure formed by four straight dykes, being all of them built over the natural terrain. The surrounding terrain is defined by agricultural terraces. The Montoliu case study is a projected off-stream reservoir located at the top of a hill with an irregular geometry. In this case, the flood propagation process is conditioned by the embankment of a highway. The Lagunilla and Segarra case studies are partially excavated off-stream reservoirs located on a ridge. Thus, depending on the break point, the water could flow down one or another valley, or both.

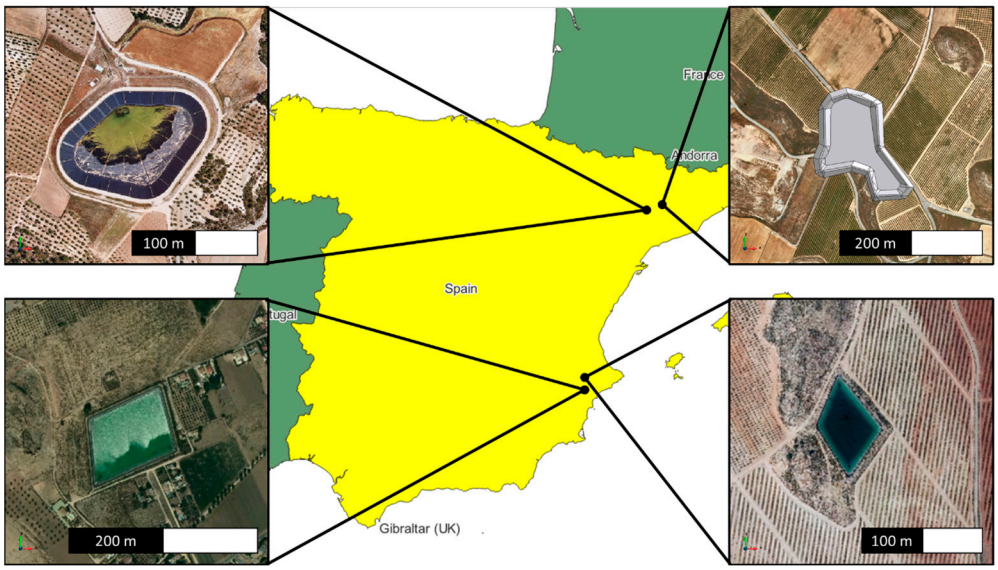

Figure 3. General location of the study sites: Segarra (**top-left**), Montoliu (**top-right**), Rubial (**bottom-left**), and Lagunilla (**bottom-right**).

The selection of the case studies was oriented to include the common typologies of embankment-made off-stream reservoirs and the different flood casuistic in case of failure. This resulted in the selection of:

- 3 already-built structures (Rubial, Lagunilla, and Segarra) and a planned one (Montoliu);
- 2 structures with all dykes above the natural terrain (Rubial and Montoliu), and 2 structures that are partially excavated in the natural terrain, but also have dykes over the natural terrain (Lagunilla and Segarra);
- the propagation of the flood may be conditioned by the proximity of a natural stream (Montoliu) or the flood may be complex and, a priori, not easily determinable (Rubial, Lagunilla and Segarra).

The authors are aware this selection cannot cover all situations worldwide. In any case, the proposed methodology can be easily extrapolated to other typologies of off-stream reservoirs (e.g., concrete, stone masonry, etc.) by including the proper breach geometry and formation characteristics of each country or region.

All geographical data needed to generate the models, such as digital terrain elevation (DTM), land uses, orthophotos and elements at risk, were obtained from the National Geographical Institute of Spain [44,45]. The DTM used in all models was a 2 m grid spacing that comes from the 2nd Coverage (2015–Present). Since the proposed methodology is independent of the topographical data, other sources, such as digital surface models (DSM), light detection and ranging (LiDAR), etc., can be utilised as well. The land uses map came from the CORINE Land Cover project [46], version 2018, and it was included in the database of Iber through the recommendations for the development of the national flood zone mapping system of Spain [47].

In all case studies, the breach formation process was considered following the specifications of the Spanish Technical Guide [40]. The breach formation process started at the beginning of the simulation (T_0 = 0 s). Only dykes that are fully exposed were selected as alignments of the crest to define the breaches. The main characteristics of the model, the off-stream reservoir, and the general values of the breach are summarized in Table 1.

Table 1. Characteristics of each study site: location, model domain, number of elements, volume of the reservoir (V), height of the dyke (H), equidistance between the generatrix axis of the breach, and number of breaches considered per model.

	X_{UTM} [m]	Y_{UTM} [m]	Zone	Domain [ha]	Num. of Elements	V [hm^3]	H [m]	Equidistance [m]	Num. of Breaches
Rubial	684,175	4,277,891	30N	395	363,375	0.13	6.70	5	136
Montoliu	300,565	4,601,762	31N	1857	421,775	0.14	5.50	10	98
Lagunilla	678,155	4,280,264	30N	398	619,102	0.06	7.50	5	54
Segarra	336,193	4,600,124	31N	646	582,086	0.16	6.83	10	56

3. Results

3.1. Probabilistic Flood Maps

The probabilistic flood maps of the case studies presented below are shown for a value of probability of exceedance of 0.01 (P[h > 0.01 m]), 0.1 (P[h > 0.1 m]), and 1 m (P[h > 1 m]) of water depth. The first criterion (P[h > 0.01 m]) is a representation of the maximum probable extent of the inundation in case of failure, and the last (P[h > 1 m]) is a representation of one of the hazard criteria of the Spanish Technical Guide, but in terms of probability. Probabilistic flood maps of other hydraulic variables (velocity, specific discharge, and water elevation) can also be obtained.

In case of the failure of the Rubial off-stream reservoir, the flood would generally extend towards the south (Figure 4a). The probability of flooding is high (above 90%) at the SE corner near the structure (Figure 4a,b). Then, the high probability area (depths greater than 0.01 and 0.1 m) is narrowed in accordance with the topography and, finally, the probability of flooding decreases downstream. Water depths above 1 m would be produced in few locations, being only appreciable near the structure and in the irrigation ditch located at the SE of the pond (Figure 4c), which generally concentrates the flow.

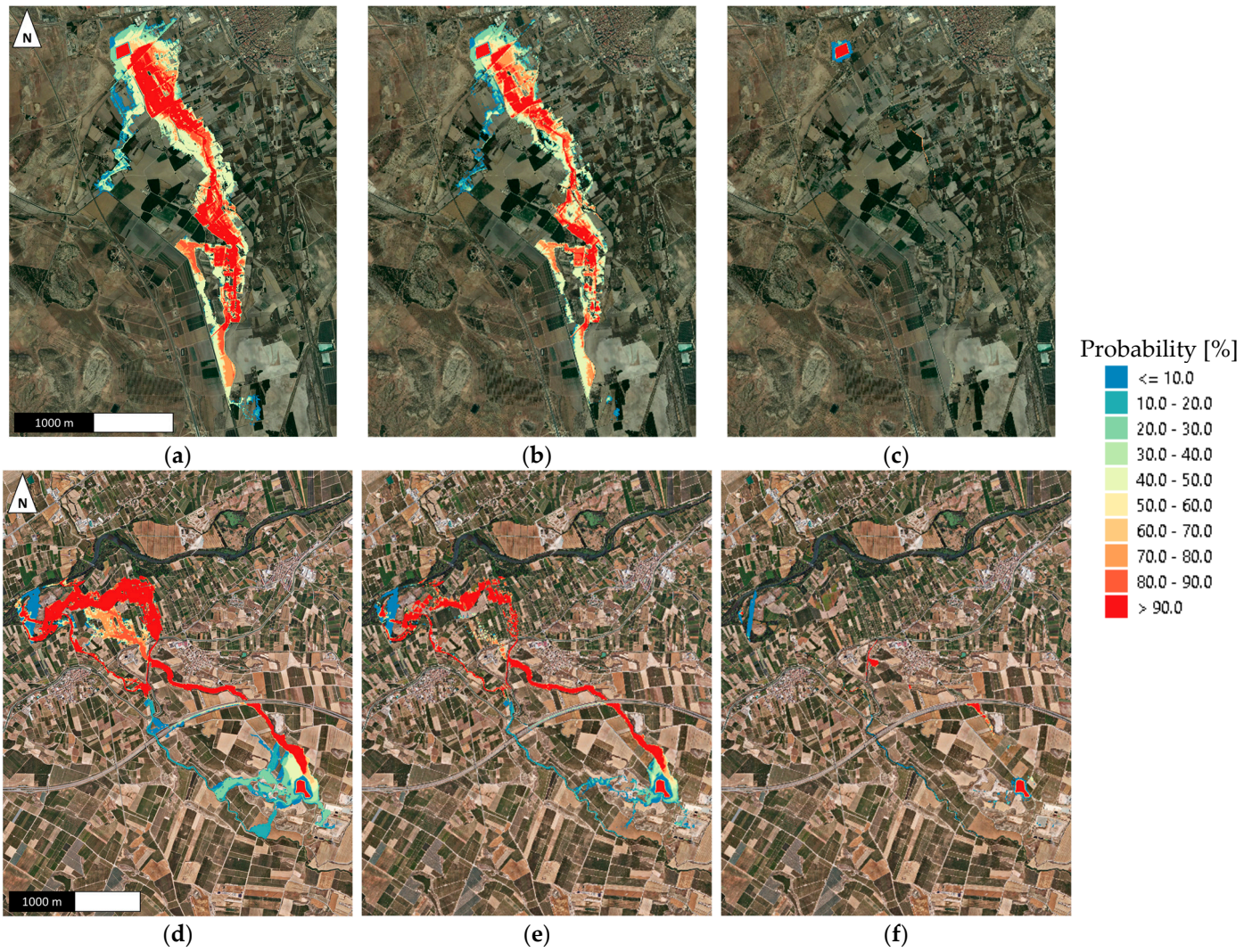

Figure 4. Maps of flood probability according to the probability of exceedance of water depth. The Rubial case: (**a**) P[h > 0.01 m], (**b**) P[h > 0.01 m], and (**c**) P[h > 1 m]. The Montoliu case: (**d**) P[h > 0.01 m], (**e**) P[h > 0.01 m], and (**f**) [h > 1 m] (background image source: [44]).

The probability of flooding in case of failure of the Montoliu off-stream reservoir shows a preference floodway towards the north, then shifting towards the NW (Figure 4d,e). The flood would generally reach the highway and the irrigation channel (Figure 4f) because the probability of exceeding 1 m of water depth is 100%, regardless of the location of break point. Contrary to what was expected, the river would not play an important role in the flood propagation process because the probability of flooding is less than 20% until the irrigation channel. At that point, the flood of the channel would generate the overtopping and the subsequent spill towards the river (with a probability above 90%). The overtopping of the channel would be produced in three points (Figure 4d) with a probability above 80% at the central part, above 90% at the southern part, and 100% at the northern part. Additionally, the flood would arrive at the highway in 100% of the cases, producing a flood over the infrastructure with a probability higher than 80%.

The flood scenarios of the Lagunilla case study generate an inundation envelope divided in two branches: one towards the north and the other to the south (Figure 5a). The probability of flooding is highly influenced by the location of the breach but, in general, the flood would be produced towards the south, with a major probability of occurrence, rather than towards the north (Figure 5b). The flow would concentrate towards the south of the gentle hill, located at the east of the pond, with a probability above 90%, while the

probability reduces to 60% towards the north with punctual locations up to 80% at the low part of the agricultural terraces. The inundation would be less probable at the north of the hill (below 50%), being the irrigation ditch reached in less than 40% of the failure cases. A probability of flooding with a water depth above 1 m is quite limited in this case, having only crossed this threshold at the pond and in its vicinity, and in very few locations in the irrigation channel (Figure 5c).

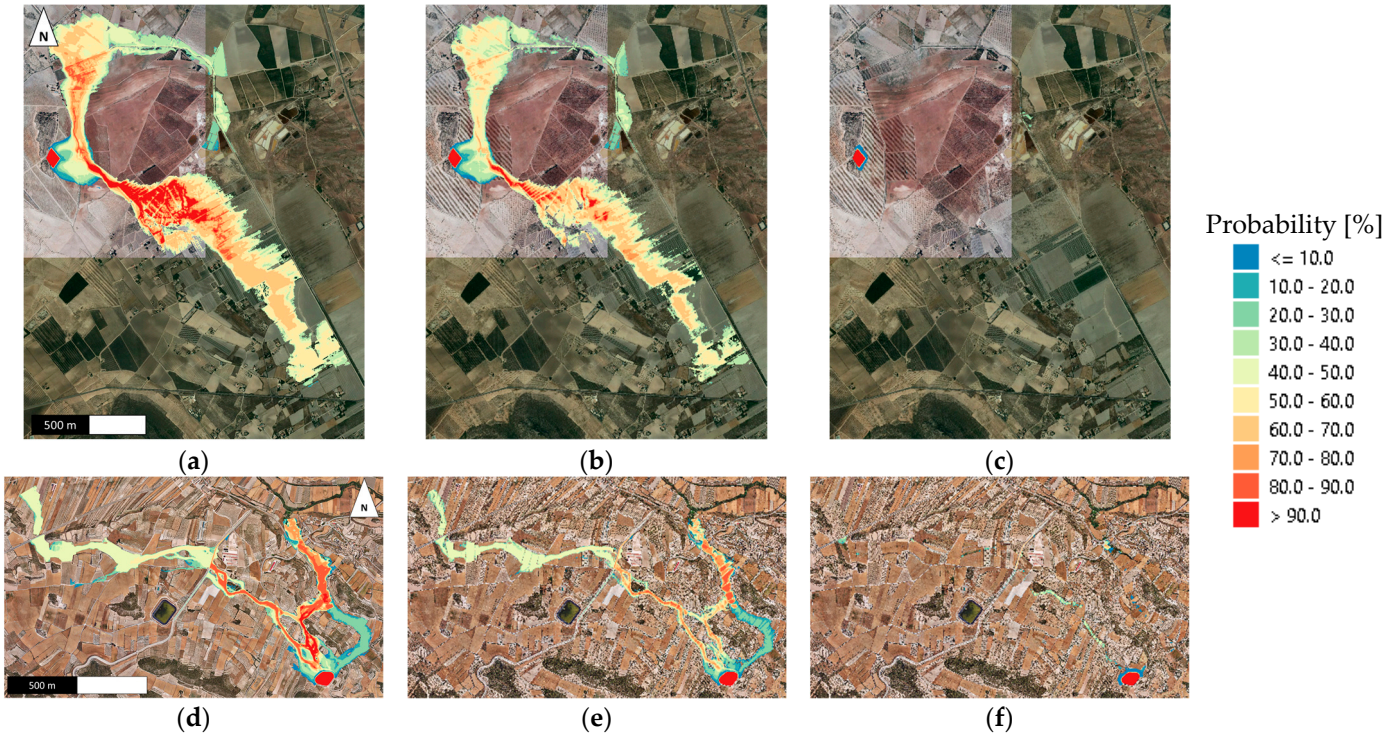

Figure 5. Maps of flood probability according to the probability of exceedance of water depth. The Lagunilla case: (**a**) P[h > 0.01 m], (**b**) P[h > 0.01 m], and (**c**) P[h > 1 m]. The Segarra case: (**d**) P[h > 0.01 m], (**e**) P[h > 0.01 m], and (**f**) P[h > 1 m] (background image source: [44]).

The failure of the Segarra off-stream would generate a complex flood probability map with several branches (Figure 5d). Despite that, the flood would generally concentrate around the central branch (north) during the first meters (probability above 90%). Then, the probability of flooding is almost identical for the northeast and northwest valleys (>80%). Only in almost 30% of the cases, the flow would reach the upper part of the NE valley (right branch). Three of the four roads located in the study area would be flooded, with a probability of 75% at a minimum. Despite the fact that the road located at the NW would be reached by the flood with almost 50% probability, it would never be flooded due to the good location and geometrical characteristics of the culvert. However, the location of the culvert for the irrigation channel is not placed correctly, and the inundation would cause an overtopping in 80% of the failure cases. Flood scenarios above 0.1 m of water depth (Figure 5e) would have a similar extension than scenarios of P[h > 0.01 m]. Water depths higher than 1 m would be produced not only near the pond, but also upstream of the roads and especially on the irrigation channel (Figure 5f).

3.2. Probabilistic Flood Hazard Assessment and Pond Classification

Danger to human life, depending on depth and velocity, has been evaluated for each case study according to the Spanish Technical Guide. That is, a 'high danger' situation in non-urban areas is defined when the water depth (h) is higher than 1 m, the flow velocity (v) is higher than 1 m/s, or the product of both variables ($h \cdot v$) is higher than 0.5 m^2/s [40]. Accounting for the potential damages caused by eventual failure or improper operation, the

structures must be classified in three categories: 'Category A' when the flood can seriously affect urban areas or essential services or cause significant material or environmental damage; 'Category B' when the flood causes significant material or environmental damage or affects a small number of dwellings; and 'Category C', the flood can cause material or environmental damage of moderate importance and only incidental loss of life. This criterion is defined for deterministic scenarios; however, it can also be applied considering the probability of threshold exceedance for these variables.

The elements at risk (EaR) considered in this analysis were houses, electric facilities, other buildings, transport infrastructures, and agricultural facilities. In the vicinity of each structure, 74, 669, 13, and 152 EaR are found in the case studies of Rubial, Montoliu, Lagunilla, and Segarra, respectively.

In the case study of Rubial, the water depth threshold ($h > 1$ m) was overcome only in 1 EaR with a probability of 2.2%. In case of the criteria of velocity ($v > 1$ m/s), 16 EaR were affected with probabilities between 3.7 and 46.8%. Only in 4 EaR was the product of both variables above the threshold ($h \cdot v > 0.5$ m^2/s). Considering that the assessment of the EaR shows 'high danger' in between 3 and 63 of the 136 scenarios simulated, the off-stream reservoir could be classified as 'Category A' with a high degree of probability independent of the break point considered.

As shown in Section 3.1, the potential flood in case of failure of the Montoliu off-stream is highly influenced by the presence of a highway and the irrigation channel. The EaR considered as 'high danger' based on the abovementioned criteria reach 80% of the failure cases analysed in the irrigation channel, and almost 65% in the highway. Other elements at risk have a lessened probability of exceeding the hydraulic variables; however, this off-stream reservoir could be classified as 'Category A' due to the potential affections to essential structures regardless of the break point.

The 13 EaR of the Lagunilla off-stream reservoir did not exceed the hydraulic threshold in any of the scenarios simulated. Thus, this structure could be classified as 'Category C' with a 100% of probability. By contrast, only 13 of the 152 EaR considered in the Segarra case study could be affected by a hypothetical failure. In three of them, the water depth and the velocity were higher than 1 m and 1 m/s, respectively, having probabilities of exceedance between 10.8 and 69.7% for the water depth, and between 9 and 69.7% for the flow velocity. Considering that, in 38 of the 56 cases simulated, the irrigation channel would be affected by the flood and the off-stream reservoir of Segarra could be classified as 'Category B' due to this EaR is considered essential.

3.3. Computational Time

The proposed methodology is integrated in the CPU and GPU versions of Iber. However, it would not be applicable in a reasonable computation timeframe without using HPC techniques, particularly general-purpose computing on a graphics processing unit (GPGPU). The benefits of using GPU instead of CPU computing are exemplified with the Rubial case study. Four mesh configurations were used to discretise the study area: 22,263, 90,239, 363,375, and 2,278,983 elements. The coarsest mesh represents only 56 calculation points, or elements, per hectare, while the finest mesh represents more than 5700 calculation points per hectare, one or two orders of magnitude above the commonly used discretization in flood studies [48]. Only four failure scenarios were calculated, corresponding each one to a breach formation at one side of the dyke of the structure, being the breach located in the middle.

Table 2 synthetises the performance of the numerical model depending on the processing unit utilised: CPU or GPU. In both cases, the computational time increases quadratically with the number of elements of the model, being necessary more than 9 days for the CPU in case of the finest mesh (more than 2.25 days per scenario). In GPU computing, this time is reduced to less than 3 h (less than 40 min per scenario). That is, using a NVIDIA® GeForce® GTX 1660 Ti device built into a laptop, the 136 scenarios of the Rubial were calculated with the second finest mesh in less than 7 h.

Table 2. Performance of the numerical model. Comparison between CPU and GPU computing.

	Elements	Area (ha)	Els./ha	Computing Time [s]	Time per Scenario [s]	Time per 1000 Els. [s]	Speed-Up
CPU	22,263	397	56	1560	390	17.5	-
	90,239		227	7140	1785	19.8	-
	363,375		913	46,800	11,700	32.2	-
	2,278,983		5727	784,848	196,212	86.1	-
GPU	22,263	397	56	120	30	1.3	13.0
	90,239		227	180	45	0.5	39.7
	363,375		913	660	165	0.5	70.9
	2,278,983		5727	9180	2295	1.0	85.5

Comparing the computing time of the GPU versus the CPU version of Iber, a speed-up of 13 was obtained for the coarsest mesh. This value increases with the number of elements, reaching a maximum of 85.5 with the finest mesh discretisation. In this case, the speed-up follows a logarithmic trend ($R^2 > 0.95$).

A scalability test was carried out comparing the number of elements and the computing time between CPU and GPU computing. The utilization of different meshes discretisation shows a constant increment in the required computing time per 1000 elements for the sequential version (CPU), while this time is almost constant, and less than 1.5 s per 1000 elements in the parallelised version (GPU). The increment of elements compared to the coarse mesh is 4 times, 16 times, and 102 times, with increments of speed-up of 3.1 times, 5.5 times, and 6.5 times respectively. Hence, the GPU version performs more efficiently than the CPU version, not only keeping the computing time per 1000 elements almost constant, but also increasing the speed-up when the number of elements of the computational domain also increases.

4. Discussion

4.1. Deterministic Flood Maps

Since the evolution of the hydraulic variables are calculated for each simulation scenario, a deterministic flood map analysis can also be performed. The results can be analysed using traditional methodologies, because maps of maximums water depths and velocities are directly provided by the numerical model, or can be exported to third party software (e.g., geographical information systems).

In the Rubial case study, in which 136 break scenarios were simulated, the main issue lies in the selection of the break point, because the perimeter of the structure is divided into four dykes oriented to the E, N, W, and S. Figure 6 shows the maximum flood extent when considering the break at the middle part on the east dyke (a), north dyke (b), west dyke (c), and south dyke (d). Despite the fact that a general trend of the flow direction towards the south is observed, the flood extension, and thus the affections to the elements at risk, notably differs. A failure towards the west would concentrate the inundation in the vicinity of the structure, while the others, especially the eastern and southern breaks, would reach maximum extension. Hence, the elements at risk would be affected to a greater or lesser extent depending on which dyke the failure was produced.

A similar situation would be produced in the Montoliu case study, because the off-stream reservoir is planned to be built over the natural terrain, but on the top of a hill. Despite a small river exists at the west, the fluid generally spreads towards the north flooding agricultural terraces and reaches a highway, first, and an irrigation channel, later (Figure 7). In several scenarios, the culvert located below the highway, at the north of the pond, would not have enough hydraulic capacity, and the water would accumulate, reaching and flowing over the road (Figure 7a–d). Only the failure of the dykes located at the south-west would reduce the amount of water flowing through the culvert (Figure 7e–f).

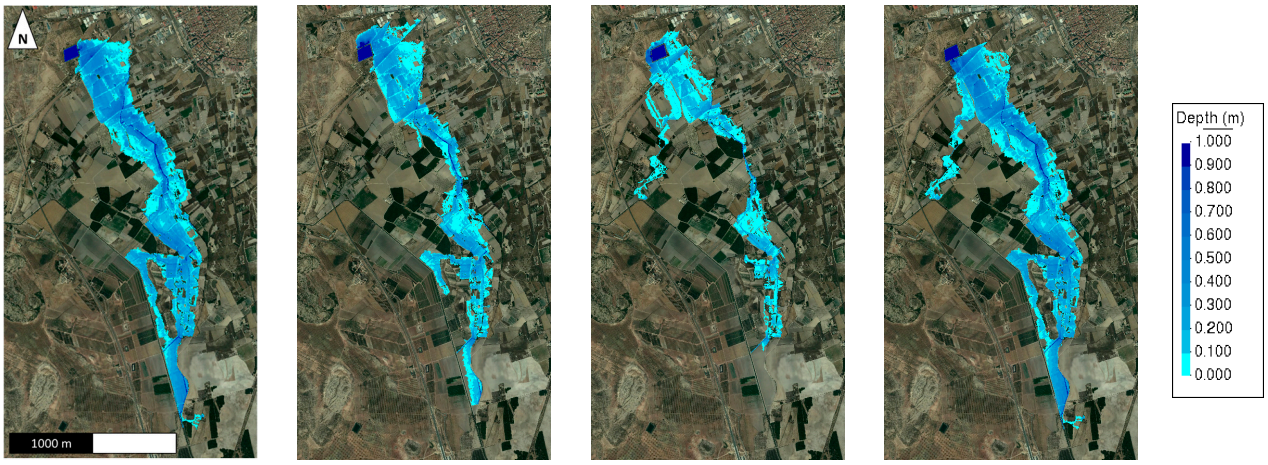

Figure 6. Rubial case study. Maximum flood extent considering the break of the (**a**) east dyke, (**b**) north dyke, (**c**) west dyke, and (**d**) south dyke. Values above 1 m are plotted in dark blue (background image source: [44]).

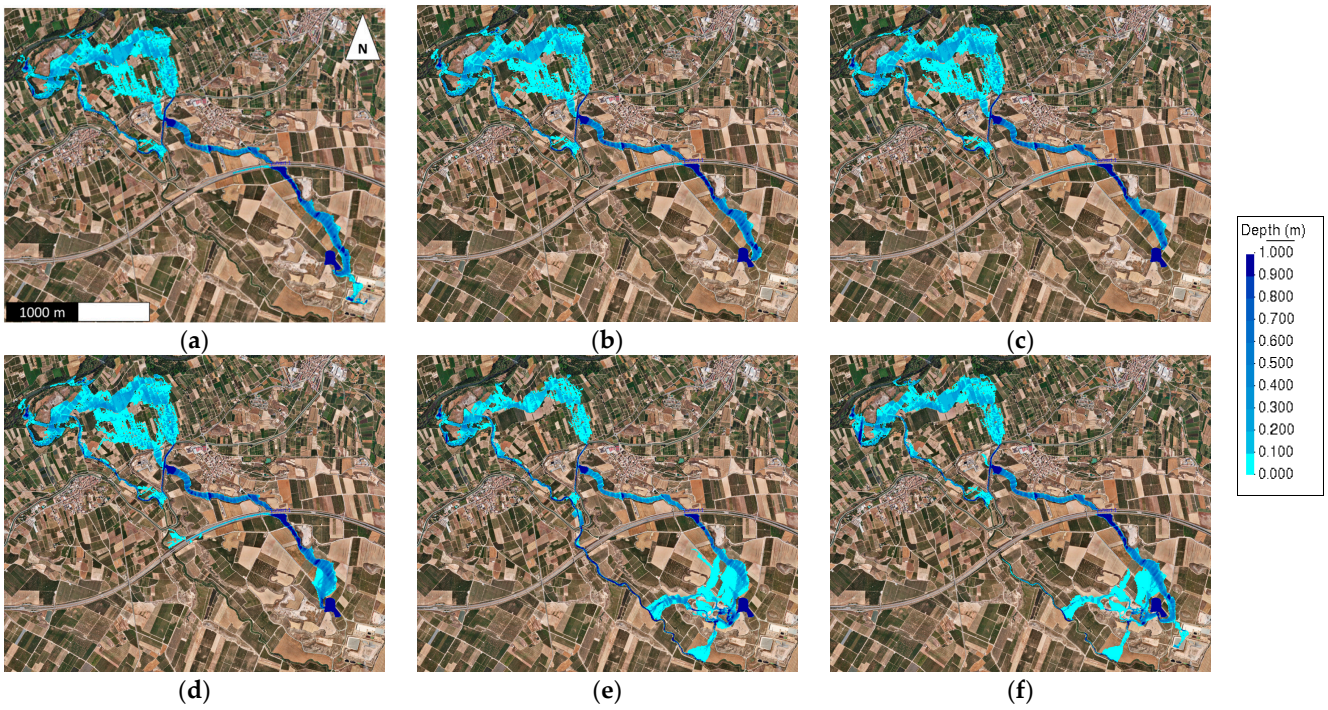

Figure 7. Montoliu case study. Maximum flood extent considering the breach (**a**) #1, (**b**) #20, (**c**) #39, (**d**) #67, (**e**) #76, and (**f**) #86.Values above 1 m are plotted in dark blue (background image source: [44]).

Lagunilla and Segarra off-stream reservoirs were partially built over the natural terrain: only one or two sides of the dyke are fully exposed. Figure 8a,b shows the maximum flood extent in Lagunilla caused by a potential failure at the medium part of the NE and SE dykes, respectively. Both inundations differ notably because a gentle hill divides the area of spill, but the SE break also floods the northern area. Breaks towards the NE would reach an irrigation ditch, meaning the flood would be partially channelled.

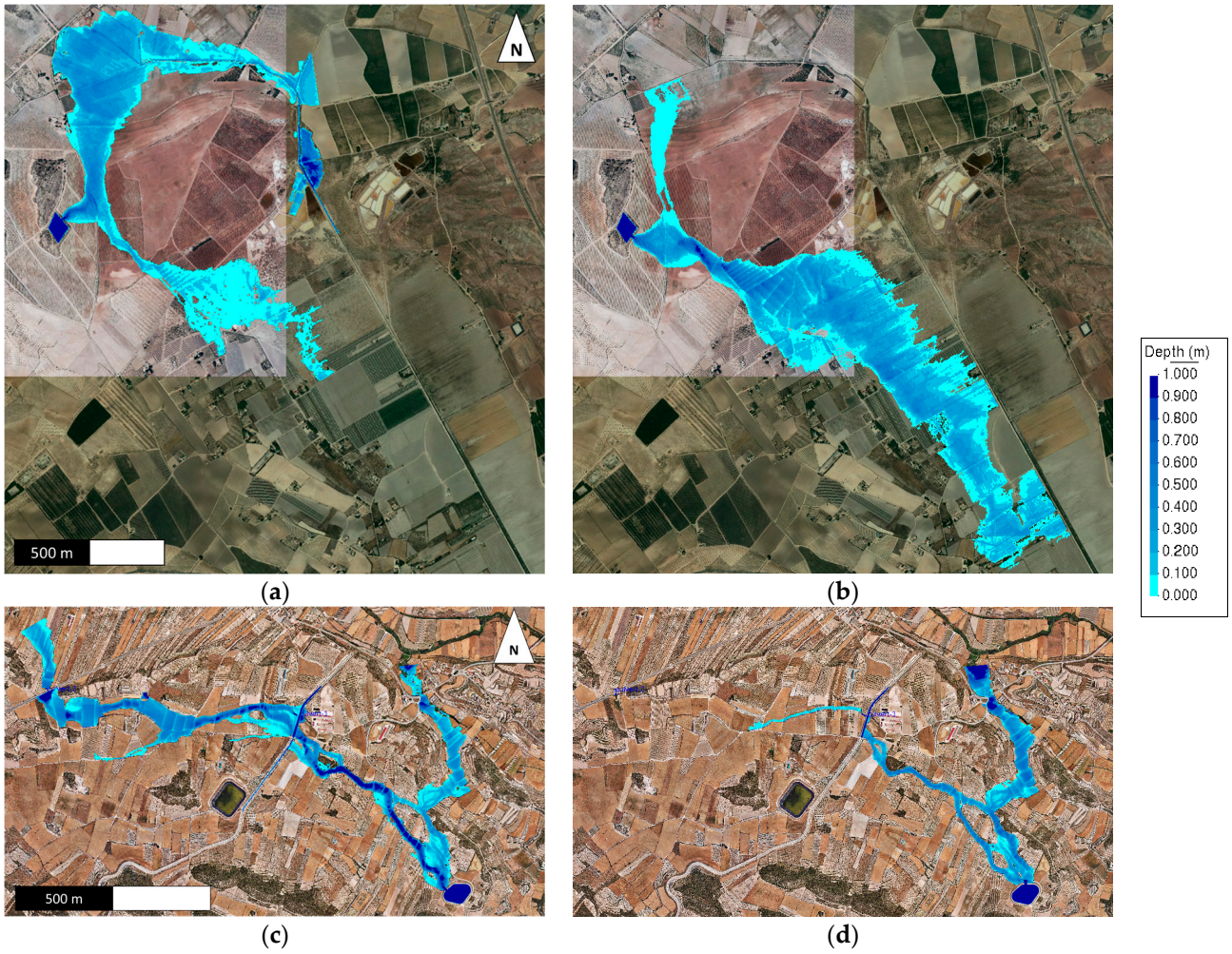

Figure 8. Maximum flood extent considering the failure of the central part of the NE dyke (**a**) and the SE dyke (**b**) of the Lagunilla case study. Maximum flood extent considering the failure of the central part of the NW dyke (**c**) and the NE dyke (**d**) of the Segarra case study. Values above 1 m are plotted in dark blue (background image source: [44]).

A similar flood process would occur in case of failure of the Segarra off-stream reservoir. Depending on the break point, the flood would propagate to a greater or lesser extent towards the NW or NE valleys. In this case, the topography is highly anthropic, mainly formed by agricultural terraces with an irrigation channel and roads, which highly condition the propagation process of the flood.

As shown in the previous cases, the selection of the break point is not trivial. A wrong selection would not provide the worst scenario in terms of maximum flood hazard: neither its extension nor hydraulic variables. Thus, a probabilistic analysis based on the stochastic generation of the break point ensures the obtaining of the global flood extent envelope that includes the worst scenario.

4.2. Which Is the Minimum Number of Breaches (Scenarios) That Would Provide Good Statistical Results?

The proposed statistical approach is based on the stochastic definition of breaches along the dykes of the off-stream reservoir. The number of breaches, or scenarios, was determined by means of an equidistance between breaches, that was 5 or 10 m depending on the case study (see Table 1). In this section, the minimum number of scenarios needed to obtain suitable statistical results is explored through the Rubial case study. The probabilistic

flood extent (P[h > 0.01 m]) is compared considering an equidistance between breaches of 5, 10, 20, and 50 m, and only 1 breach per dyke.

The histograms of the probability, grouped in ranges of 10%, are summarised in Table 3. As expected, the flood extent increases with the number of breaches considered. By contrast, the frequency of 100% slightly increases when the number of scenarios decreases, being 3205 for 5 m equidistance, while it is 3311 for 1 breach per side. The histograms are similar for equidistances of 5, 10, and 20 m, with particular differences in the upper part (>70%) for the 20 m equidistance.

Table 3. Histogram of probability. Number of elements per range of probability for P[h > 0.01 m].

Range of Probability [%].	1breach X 1side	1breach X 50 m	1breach X 20 m	1breach X 10 m	1breach X 5 m
0–10	0	23,649	34,058	37,686	39,018
10–20	0	11,708	17,618	22,416	22,220
20–30	58,418	23,303	43,302	38,590	36,576
30–40	0	71,261	29,639	28,431	29,373
40–50	183,439	109,808	143,468	148,079	146,582
50–60	0	32,592	22,850	18,556	21,162
60–70	0	30,275	12,812	15,339	16,539
70–80	139,938	105,684	120,138	47,763	44,457
80–90	0	5858	6513	78,722	80,043
90–100	175,786	175,832	175,622	175,642	175,904
Total	557,581	589,970	606,020	611,224	611,874

The three major frequencies concentrate in 40–50, 80–90, and 90–100% for the 5 and 10 m equidistance. This trend changes completely for 20 and 50 m equidistance and 1 breach per side, especially for high flood probabilities (>70%). In these cases, the range between 70 and 80% concentrates the third major frequency with the same order of magnitude than the second and the first. These values clearly differ from the results obtained with the scenarios of an equidistance of 5 and 10 m, particularly in the range 80–90%, in which it is the third major frequency, while it is the ninth for the other scenarios. As expected, the scenario defined as a breach per side only has frequencies in 25, 50, 75, and 100% of probability of exceedance of the hydraulic variable, frequencies of 50 and 100% being the same order of magnitude as the rest of scenarios.

As shown, scenarios with equidistances between breaches of 5 and 10 m provide similar results. In this case, using half the distance between breaches only increases the flood extent by about 0.1%, thus both equidistances are statistically significant and consistent. Despite an equidistance of 20 m between breaches providing similar results in comparison with 10 and 5 m equidistance, the appreciable differences in the lower and upper part of the histogram could make the results unsuitable. This fact is reproduced in the other case studies, regardless of the location of the off-stream reservoir and the generation of branches of inundation.

4.3. Limiting the Calculation Domain

As mentioned before, one of the main issues for practitioners when dealing with off-stream reservoir failure studies is the location of the breach that generates the worst results in terms of flood hazard. In this regard, the definition of the calculation domain is also challenging because the flood extent is, a priori, unknown. This is especially complex to determine in highly anthropic topographies, where off-stream reservoirs are commonly located to supply water for agricultural purposes.

This problem is commonly by-passed—not fully solved—by defining a sufficiently large calculation domain. With that, the numerical model is not optimised, and a huge number of elements are unnecessarily used to discretise the computational domain. A major number of elements generally implies greater calculation times, despite using HPC

techniques [35]. Thus, a previous analysis should be required with the aim of reducing the calculation domain, the total number of elements strictly necessary and, as a consequence of that, the global computational time.

The methodology presented in Section 2.2 to generate the stochastic scenarios can also be used to determine an optimised computation domain utilising, for that purpose, a coarse mesh. In this case, the whole simulation process will run in a few minutes, even in large computational domains. Once the simulation process ends, a flood map corresponding to a probability of over 0.01 m of water depth, or less, roughly provides the envelope of the flood extent. The definitive and optimised computational domain can be obtained by applying a buffer to this preliminary flood area.

This technique was utilised for all case studies presented herein. For example, in the Segarra case study, an original model was utilised to simulate the flood propagation, discretising a study area equivalent to the extension of the topographic sheet (2267 ha). Applying the proposed methodology and a buffer of 100 m, the study area was reduced to 646 ha. The first model built for the Lagunilla case had 676 ha and, once fine-tuned, the total area of the calculation domain reduced to 398 ha (also with a buffer of 100 m). Therefore, this approach can also be useful for optimising the numerical model, reducing the number of elements to half or less and, as proved in Section 3.3, also the global computational time.

4.4. Fine-Tuning Hazard and Risk Criteria to Assess the Potential Flood Damage in Roadways

The classification of off-stream reservoirs should not be overly complex. The release of the current Spanish Technical Guide [40] in 2021, which replaced the old version of 1996 [49], is a step forward, despite it being mainly oriented—and defined—for dams. Although other technical documents are, a priori, not necessary to interpret the current guideline [50], the classification process defined in 1996, and also in 2021, admits the development of new strategies to carry out the flood hazard assessment for dams and ponds [51].

The flood hazard criterion in the case of non-urban areas was accommodated to follow the hazard criteria in case of fluvial inundations [52]. However, the assessment of the potential flood damage when roadways might be exposed is less defined, especially the hazard criteria [53].

To that end, Martínez-Gomariz et al. [53] present a new methodology to assess potential flood damage to roads in the case of dams or ponds failure. The safety of the vehicle occupants is pointed out when the stability is lost in case of flood. They propose not only the application of a proper hazard criterion based on the stability of the vehicle [54], but also a vulnerability criterion to floods according to the exposure (minimum and maximum expected number of vehicles), the sensitivity (age of the vehicles), and the number of occupants per vehicle.

Keeping in mind that the category of an off-stream reservoir might depend on the assessment of hazard in roadways, such as in the Montoliu and Segarra case studies, this criterion could fine-tune the potential flood damage assessment in case of failure. The floodable road length is a critical parameter [54], and it could be underestimated if a deterministic flood assessment is conducted.

With the proposed probabilistic approach, the flood envelop can be directly obtained, which considers any break point along the dyke(s) of the off-stream reservoir. Hence, both methodologies are complementary and may fine-tune the current flood hazard assessment in case of an off-stream reservoir failure.

4.5. A Machine Learning Approach for Estimating the High-Risk Areas

As stated previously, the Spanish Technical Guide allows the utilisation of well-justified alternative methodologies that help in the classification process function of the potential risk in case of failure. That is, for example, the use of machine learning (ML), a common technique used to predict the behaviour of structures [55,56], morphodyncamic evolution [57], hydrological purposes [58], the flood extent [59], and the peak discharge due to breaching of embankment dams [60], among others.

Silva-Cancino et al. [61] presented a methodology based on ML to identify risk zones at any point in the vicinity of an off-stream reservoir. A ML-based surrogate model was trained with data obtained from 1200 two-dimensional hydraulic synthetic cases. For each model, 200 elements at risk were randomly distributed within the computational domain. The hydraulic variables were then extracted, providing a database of 240,000 points classified as 'low danger' and 'high danger' according to the Spanish Technical Guide for non-urban areas. The ML predictive model is based on the random forest classification algorithm and provides a pre-classification of the off-stream reservoir (A, B or C) accounting for the topographical data, the location of the elements at risk, and some geometrical data.

The random forest classifier algorithm uses class probabilities to estimate the correct predicted class in each tree and in the overall prediction [62]. That is, an element at risk is taken as 'high danger' if the class probability is higher than the probability threshold (defined as 0.5). A probability above this threshold, but close to 1, means a more reliable prediction of the ML model.

The class probability also applies to a complete study area, such as was performed in the Rubial case study. Probabilities between 50 and 60% were obtained in most of the areas predicted as 'high danger' in the vicinity of the structure, while more reliable predictions were observed in the irrigation ditch with values above 60% (Figure 9a). By contrast, the proposed methodology provides a map of the probability of 'high danger' in case of stochastic failure of the off-stream reservoir (Figure 9b). Both methodologies present a similar spatial distribution of the results, with high values near the pond and in the irrigation ditch.

(**a**) (**b**)

Figure 9. Rubial case study: (**a**) class probability associated to the locations considered as 'high danger' by the ML model and a break point at the middle part of the south dyke, and (**b**) probability of 'high danger' obtained by the proposed methodology (background image source: [44]).

The results of the proposed methodology model are richer and have higher resolution than ML-based approaches. For example, from the 74 elements at risk of this case study, 4 of them have a probability of being 'high danger' between 40 and 50%, 3 between 30 and 40%, 7 between 20 and 30%, 2 between 10 and 20%, and the other less than 10%. That is, in at least 40 of the 136 simulated cases, seven elements at risk were classified as 'high danger'. Thus, the structure would be classified as 'Category A' with a probability greater than 30%.

The ML-based approach provides the 'high danger' class with a certain degree of uncertainty. That is, how reliable are the estimated results. By contrast, the map of

probability of the proposed methodology is per se a reliable result because a probability greater than 0% means that there is, at least, one scenario in which 'high danger' is obtained in an element at risk.

5. Conclusions

One of the main issues faced by practitioners when classifying an off-stream reservoir according to its potential damage in case of failure is the establishment of the breaking point location. To that end, a novel methodology has been developed to cover all possibilities, and that serves to carry out a probabilistic approach for off-stream reservoir failure flood hazard assessment.

A stochastic generation of breaches along the dyke of the off-stream reservoir is defined, the results being statistically significant and consistent with an equidistance of 5 and 10 m between breaches. Then, an in-cascade calculation process simulates each breach formation and the flood propagation process in the same model. Due to the large number of simulations, the results can be analysed from a probabilistic point of view, thereby generating maps of probability of inundation in case of a potential failure of the structure.

The proposed methodology allows for the direct determination of the global envelope of the flood extent, using a low value for the probability of exceedance threshold of water depth (e.g., P[h > 0.01 m]). Thereby, the simulation of the worst break scenario is ensured from a purely hydraulic point of view. However, the global probability of flooding also depends on the structural strength of the dyke.

With the proposed methodology, it is possible to obtain the deterministic flood maps of all scenarios calculated in the same model. The methodology also allows the determination of an optimised computation domain for more detailed simulations, e.g., by using a coarse mesh and a buffer of the resulting enveloping flood extent. The methodology can be extrapolated to other typologies of off-stream reservoirs, other kinds of breaches, and adapted to other safety regulations. Thereby, it is an open and easily-adaptable methodology, the results of which are less dependent on the practitioners and can provide a more homogenous framework for water authorities or agencies when evaluating dam-break flood-hazard studies.

The implementation of the breach formation process in a parallelised code, jointly with the flood propagation process, allows the simulation of high-resolution numerical models in a reasonable computation timeframe. The integration of the probabilistic approach, together with the classical deterministic approach, expands the functionalities of the numerical tool and attempts to solve the main issue, when dealing with the assessment and classification, according to their downstream potential damage.

Author Contributions: Conceptualization, M.S.-R. and E.B.; methodology, M.S.-R., E.B., N.S.-C. and F.S.; software, M.S.-R., E.B. and D.L.-G.; formal analysis, M.S.-R., E.B. and F.S.; resources, E.B., N.S.-C., F.S., D.L.-G. and E.M.-G.; data curation, E.B., N.S.-C., F.S., D.L.-G. and E.M.-G.; writing—original draft preparation, M.S.-R. and N.S.-C.; writing—review and editing, E.B., F.S., D.L.-G. and E.M.-G. All authors have read and agreed to the published version of the manuscript.

Funding: This work was partially funded by the Spanish Ministry of Science, Innovation and Universities through the Projects ACROPOLIS (RTC2019-007343-5), and DOLMEN (PID2021-122661OB-I00), as well as by the Spanish Ministry of Economy and Competitiveness, through the Severo Ochoa Programme for Centres of Excellence in R & D (CEX2018-000797-S), and by the Generalitat de Catalunya through the CERCA Program.

Institutional Review Board Statement: Not applicable.

Informed Consent Statement: Not applicable.

Data Availability Statement: Data available in a publicly accessible repository that does not issue DOIs.

Acknowledgments: The authors thank the Junta Central de Usuarios del Vinalopó, L'Alacantí y Consorcio de Aguas de la Marina Baja (JCU), the Comunidad de Regantes de Huerta y Partidas

de Villena and ARVUM, who provided us with information on the 'Rubial' and 'Lagunilla' case studies. Finally, thanks to V.J. Richart, a technician from JCU, for his interest in the project and its developments.

Conflicts of Interest: The authors declare no conflict of interest. The funders had no role in the design of the study; in the collection, analyses, or interpretation of data; in the writing of the manuscript; or in the decision to publish the results.

References

1. ISDR. *Global Assessment Report on Disaster Risk Reduction*; United Nations: Geneva, Switzerland, 2009; ISBN 978-92-1-332019-8.
2. Kron, W. Flood Risk = Hazard + Values + Vulnerability. *Water Int.* **2005**, *30*, 58–68. [CrossRef]
3. La Salandra, M.; Roseto, R.; Mele, D.; Dellino, P.; Capolongo, D. Probabilistic hydro-geomorphological hazard assessment based on UAV-derived high-resolution topographic data: The case of Basento river (Southern Italy). *Sci. Total Environ.* **2022**, *842*, 156736. [CrossRef] [PubMed]
4. Casas, A.; Aurell, M.; Revuelto, C.; Calvín, P.; Simón, J.L.; Pueyo, Ó.; Pocoví, A.; Marcén, M. Geological hazards (seismicity and catastrophic flooding) associated with the Mularroya dam (Grío river, Zaragoza province, Spain). *Rev. Soc. Geol. Espana* **2017**, *30*, 51–64.
5. Palau-Ibars, A.; Batalla, R.J.; Rosico, E.; Meseguer, A.; Vericat, D.; Palau, A.; Batalla, R.J.; Rosico, E.; Meseguer, A.; Vericat, D. Management of water level and design of flushing floods for environmental river maintenance downstream of the Riba-Roja reservoir (lower Ebro River. NE Spain). In Proceedings of the HYDRO 2004—A New Era for Hydropower, Porto, Portugal, 18–20 October 2004.
6. Mazzoleni, M.; Dottori, F.; Cloke, H.L.; Di Baldassarre, G. Deciphering human influence on annual maximum flood extent at the global level. *Commun. Earth Environ.* **2022**, *3*, 262. [CrossRef]
7. Anees, M.T.; Abdullah, K.; Nordin, M.N.M.; Rahman, N.N.N.A.; Syakir, M.I.; Kadir, M.O.A. One- and Two-Dimensional Hydrological Modelling and Their Uncertainties. In *Flood Risk Management*; InTech: London, UK, 2017; pp. 11, 221–244.
8. Singh, R.B.; Singh, S. Rapid urbanization and induced flood risk in Noida, India. *Asian Geogr.* **2011**, *28*, 147–169. [CrossRef]
9. Roy, P.; Pal, S.C.; Arabameri, A.; Rezaie, F.; Chakrabortty, R.; Chowdhuri, I.; Saha, A.; Malik, S.; Das, B. Climate and land use change induced future flood susceptibility assessment in a sub-tropical region of India. *Soft Comput.* **2021**, *25*, 5925–5949. [CrossRef]
10. Brath, A.; Montanari, A.; Moretti, G. Assessing the effect on flood frequency of land use change via hydrological simulation (with uncertainty). *J. Hydrol.* **2006**, *324*, 141–153. [CrossRef]
11. Schultz, B. Water management and flood protection of the polders in the Netherlands under the impact of climate change and man-induced changes in land use. *J. Water Land Dev.* **2008**, *12*, 71–94. [CrossRef]
12. Adamo, N.; Al-Ansari, N.; Sissakian, V.; Laue, J.; Knutsson, S. Dam Safety: Hazards Created by Human Failings and Actions. *J. Earth Sci. Geotech. Eng.* **2020**, *11*, 65–107. [CrossRef]
13. Davies, M.P.; Martin, T.E.; Lighthall, P. Mine Tailings Dams: When Things Go Wrong. In Proceedings of the ASDSO Conference Papers, Tailing Dams 2000, Las Vegas, NV, USA, 28–30 March 2000; p. 13.
14. Kryžanowski, A.; Brilly, M.; Rusjan, S.; Schnabl, S. Review Article: Structural flood-protection measures referring to several European case studies. *Nat. Hazards Earth Syst. Sci.* **2014**, *14*, 135–142. [CrossRef]
15. Sanz-Ramos, M.; Martí-Cardona, B.; Bladé, E.; Seco, I.; Amengual, A.; Roux, H.; Romero, R. NRCS-CN Estimation from Onsite and Remote Sensing Data for Management of a Reservoir in the Eastern Pyrenees. *J. Hydrol. Eng.* **2020**, *25*, 05020022. [CrossRef]
16. Roux, H.; Amengual, A.; Romero, R.; Bladé, E.; Sanz-Ramos, M. Evaluation of two hydrometeorological ensemble strategies for flash-flood forecasting over a catchment of the eastern Pyrenees. *Nat. Hazards Earth Syst. Sci.* **2020**, *20*, 425–450. [CrossRef]
17. Wood, E. An analysis of flood levee reliability. *Water Resour. Res.* **1977**, *13*, 665–671. [CrossRef]
18. Vahedifard, F.; AghaKouchak, A.; Ragno, E.; Shahrokhabadi, S.; Mallakpour, I. Lessons from the Oroville dam. *Science* **2017**, *355*, 1139–1140. [CrossRef]
19. Sahoo, D.; Yazdi, M.Y.; Owen, J.S.; White, S.A. *The Basics of Irrigation Reservoirs for Agriculture*; Clemson (SC): ClemsonCooperative Extension, Land-Grant Press by Clemson Extension, 2021 Oct. LGP 1121. Available online: https://lgpress.clemson.edu/publication/the-basics-of-irrigation-reservoirs-for-agriculture/ (accessed on 21 April 2023).
20. Sanz-Ramos, M.; Bladé, E.; Dolz, J.; Sánchez-Juny, M. Revisiting the Hydraulics of the Aznalcóllar Mine Disaster. *Mine Water Environ.* **2022**, *41*, 335–356. [CrossRef]
21. Bladé, E.; Sanz-Ramos, M.; Dolz, J.; Expósito-Pérez, J.; Sánchez-Juny, M. Modelling flood propagation in the service galleries of a nuclear power plant. *Nucl. Eng. Des.* **2019**, *352*, 110180. [CrossRef]
22. Nguyen, D.T. Operating Multi-Purpose Reservoirs in the Red River Basin: Hydropower Benefit Optimization in Conditions Ensuring Enough Water for Downstream Irrigation. *Sustainability* **2023**, *15*, 5444. [CrossRef]
23. Sanz-Ramos, M.; Bladé, E.; Dolz, J.; Sánchez-Juny, M. El desastre de Aznalcóllar: ¿lodos o aguas ácidas? *Ing. Agua* **2021**, *25*, 229. [CrossRef]
24. Wishart, M.J.; Ueda, S.; Pisaniello, J.D.; Tingey-Holyoak, J.L.; Lyon, K.N.; Boj-García, E. *Laying the Foundations; Laying the Foundations: A Global Analysis of Regulatory Frameworks for the Safety of Dams and Downstream Communities: A Global Analysis of*

Regulatory Frameworks for the Safety of Dams and Downstream Communities. Sustainable Infras; World Bank: Washington, DC, USA, 2020. Available online: https://openknowledge.worldbank.org/entities/publication/83fd9d00-3207-55fd-8a69-81094c930110 (accessed on 15 May 2023).
25. Albano, R.; Mancusi, L.; Adamowski, J.; Cantisani, A.; Sole, A. A GIS Tool for Mapping Dam-Break Flood Hazards in Italy. *ISPRS Int. J. Geo-Inf.* **2019**, *8*, 250. [CrossRef]
26. Rodrigues, A.S.; Santos, M.A.; Santos, A.D.; Rocha, F. Dam-Break Flood Emergency Management System. *Water Resour. Manag.* **2002**, *16*, 489–503. [CrossRef]
27. Ahmadisharaf, E.; Mahmud-Bhuyian, M.N.; Kalyanapu, A. Impact of spatial resolution on downstream flood hazard due to dam break events using probabilistic flood modeling. In Proceedings of the 5th Dam Safety Conference, Association of State Dam Safety Officials Annual Conference 2013, Dam Safety 2013, Providence, RI, USA, 8–12 September 2013; Volume 1, pp. 14, 263–276.
28. Rizzo, C.; Maranzoni, A.; D'Oria, M. Probabilistic mapping and sensitivity assessment of dam-break flood hazard. *Hydrol. Sci. J.* **2023**, *68*, 700–718. [CrossRef]
29. Bello, D.; Alcayaga, H.; Caamaño, D.; Pizarro, A. Influence of Dam Breach Parameter Statistical Definition on Resulting Rupture Maximum Discharge. *Water* **2022**, *14*, 1776. [CrossRef]
30. Bladé, E.; Cea, L.; Corestein, G. Numerical modelling of river inundations. *Ing. Agua* **2014**, *18*, 68. (In Spanish) [CrossRef]
31. Bladé, E.; Cea, L.; Corestein, G.; Escolano, E.; Puertas, J.; Vázquez-Cendón, E.; Dolz, J.; Coll, A. Iber: River flow numerical simulation tool. *Rev. Int. Métodos Numéricos Para Cálculo Y Diseño Ing.* **2014**, *30*, 1–10. (In Spanish) [CrossRef]
32. Cea, L.; Bladé, E. A simple and efficient unstructured finite volume scheme for solving the shallow water equations in overland flow applications. *Water Resour. Res.* **2015**, *51*, 5464–5486. [CrossRef]
33. Ruiz-Villanueva, V.; Bladé, E.; Sánchez-Juny, M.; Marti-Cardona, B.; Díez-Herrero, A.; Bodoque, J.M. Two-dimensional numerical modeling of wood transport. *J. Hydroinform.* **2014**, *16*, 1077. [CrossRef]
34. Sanz-Ramos, M.; Bladé, E.; Palau, A.; Vericatl, D.; Ramos-Fuertes, A. IberHABITAT: Assessment of Physical Habitat Suitability and Weighted Usable Area for fishes. Application in the Eume River. *Ribagua* **2019**, *6*, 158–167. [CrossRef]
35. Sanz-Ramos, M.; López-Gómez, D.; Bladé, E.; Dehghan-Souraki, D. A CUDA Fortran GPU-parallelised hydrodynamic tool for high-resolution and long-term eco-hydraulic modelling. *Environ. Model. Softw.* **2023**, *161*, 105628. [CrossRef]
36. Cea, L.; Bermúdez, M.; Puertas, J.; Bladé, E.; Corestein, G.; Escolano, E.; Conde, A.; Bockelmann-Evans, B.; Ahmadian, R. IberWQ: New simulation tool for 2D water quality modelling in rivers and shallow estuaries. *J. Hydroinform.* **2016**, *18*, 816–830. [CrossRef]
37. Bladé, E.; Sánchez-Juny, M.; Arbat, M.; Dolz, J. Computational Modeling of Fine Sediment Relocation Within a Dam Reservoir by Means of Artificial Flood Generation in a Reservoir Cascade. *Water Resour. Res.* **2019**, *55*, 3156–3170. [CrossRef]
38. Sanz-Ramos, M.; Olivares, G.; Bladé, E. Experimental characterization and two-dimensional hydraulic-hydrologic modelling of the infiltration process through permeable pavements. *Rev. Int. Métodos Numéricos Para Cálculo y Diseño Ing.* **2022**, *38*, 14. [CrossRef]
39. Sanz-Ramos, M.; Bladé, E.; Torralba, A.; Oller, P. Saint Venant's equations for dense-snow avalanche modelling. *Ing. Agua* **2020**, *24*, 65–79. (In Spanish) [CrossRef]
40. MITECO. *Technical Guide for the Classification of Dams*; Ministerio para la transición ecológica y el reto demográfico (MITECO): Madrid, Spain, 2021. (In Spanish)
41. Sánchez Romero, F.J. *Safety Criteria in Earthen Ponds for Irrigation*; Universitat Politècnica de València: Valencia, Spain, 2014. (In Spanish)
42. Morales-Hernández, M.; Sharif, M.B.; Kalyanapu, A.; Ghafoor, S.K.; Dullo, T.T.; Gangrade, S.; Kao, S.-C.; Norman, M.R.; Evans, K.J. TRITON: A Multi-GPU open source 2D hydrodynamic flood model. *Environ. Model. Softw.* **2021**, *141*, 105034. [CrossRef]
43. Kheirkhah Gildeh, H.; Halliday, A.; Arenas, A.; Zhang, H. Tailings Dam Breach Analysis: A Review of Methods, Practices, and Uncertainties. *Mine Water Environ.* **2021**, *40*, 128–150. [CrossRef]
44. IGN. Ortofotos E Imágenes Satélite. Available online: http://centrodedescargas.cnig.es/CentroDescargas/catalogo.do?Serie=PNOAH (accessed on 6 April 2021).
45. IGN. Digital Elevation Models. Available online: http://centrodedescargas.cnig.es/CentroDescargas/ (accessed on 26 April 2022).
46. EEA. *CORINE Land Cover Technical Guide—Addendum 2000*; Technical Report No. 40; European Enviromental Agency: Copenhague, Denmark, 2000.
47. MAGRAMA. *Methodological Guide for the Development of the National Flood Zone Mapping System*; Ministerio de Medio Ambiente y Medio Rural y Marino, Gobierno de España: Madrid, Spain, 2011. ISBN 978-84-491-1136-5. (In Spanish)
48. Sanz-Ramos, M.; Bladé, E.; Escolano, E. Optimization of the Floodplain Encroachment calculation with hydraulic criteria. *Ing. Agua* **2020**, *24*, 203. (In Spanish) [CrossRef]
49. MMA. *Techincal Guide for the Classification of Dams Function of the Potential Risk*; Ministerio de Medio Ambiente. Dirección General de Obras Hidráulicas y Calidad de las Aguas: Madrid, Spain, 1996. (In Spanish)
50. ACA. *Criteris D'interpretació de la Guia Tècnica de Classificació de Preses en Funció del Risc Potencial*; Agència Catalana de l'Aigua, Generalitat de Catalunya: Barcelona, Spain, 2014.
51. Sanz-Ramos, M.; Olivares Cerpa, G.; Bladé i Castellet, E. Metodología para el análisis de rotura de presas con aterramiento mediante simulación con fondo móvil. *Ribagua* **2019**, *6*, 138–147. [CrossRef]

52. *BOE-A-2008-755 Real Decreto 9/2008, de 11 de enero, por el que se modifica el Reglamento del Dominio Público Hidráulico, aprobado por el Real Decreto 849/1986, de 11 de abril*; Boletín Estado núm. 14 16 enero 2008; Ministerio de la Presidencia: Madrid, Spain, 2008; Volume 9, pp. 3141–3149.
53. Martínez-Gomariz, E.; Barbero, C.; Sanchez-Juny, M.; Forero-Ortiz, E.; Sanz-Ramos, M. Dams or ponds classification based on a new criterion to assess potential flood damage to roads in case of failure. *Nat. Hazards* **2023**, *117*, 625–653. [CrossRef]
54. Martínez-Gomariz, E.; Gómez, M.; Russo, B.; Djordjević, S. A new experiments-based methodology to define the stability threshold for any vehicle exposed to flooding. *Urban Water J.* **2017**, *14*, 930–939. [CrossRef]
55. Salazar, F.; Toledo, M.A.; Oñate, E.; Morán, R. An empirical comparison of machine learning techniques for dam behaviour modelling. *Struct. Saf.* **2015**, *56*, 9–17. [CrossRef]
56. Salazar, F.; Toledo, M.T.; Oñate, E.; Suárez, B. Interpretation of dam deformation and leakage with boosted regression trees. *Eng. Struct.* **2016**, *119*, 230–251. [CrossRef]
57. Bonakdari, H.; Moradi, F.; Ebtehaj, I.; Gharabaghi, B.; Sattar, A.A.; Azimi, A.H.; Radecki-Pawlik, A. A Non-Tuned Machine Learning Technique for Abutment Scour Depth in Clear Water Condition. *Water* **2020**, *12*, 301. [CrossRef]
58. Zhu, R.; Yang, L.; Liu, T.; Wen, X.; Zhang, L.; Chang, Y. Hydrological Responses to the Future Climate Change in a Data Scarce Region, Northwest China: Application of Machine Learning Models. *Water* **2019**, *11*, 1588. [CrossRef]
59. Diez-Herrero, A.; Garrote, J. Flood risk analysis and assessment, applications and uncertainties: A bibliometric review. *Water* **2020**, *12*, 2050. [CrossRef]
60. Hooshyaripor, F.; Tahershamsi, A.; Behzadian, K. Estimation of peak outflow in dam failure using neural network approach under uncertainty analysis. *Water Resour.* **2015**, *42*, 721–734. [CrossRef]
61. Silva-Cancino, N.; Salazar, F.; Sanz-Ramos, M.; Bladé, E. A Machine Learning-Based Surrogate Model for the Identification of Risk Zones Due to Off-Stream Reservoir Failure. *Water* **2022**, *14*, 2416. [CrossRef]
62. Bostrom, H. Estimating class probabilities in random forests. In Proceedings of the Sixth International Conference on Machine Learning and Applications (ICMLA 2007), Cincinnati, OH, USA, 13–15 December 2007; Institute of Electrical and Electronic Engineering (IEEE): Piscataway, NJ, USA, 2007; pp. 211–216.